The Plant Cell, Vol. 25: 2171–2186, June 2013, www.plantcell.org 

# The Caspase-Related Protease Separase (EXTRA SPINDLE POLES) Regulates Cell Polarity and Cytokinesis in *Arabidopsis*[C][W]

**Panagiotis N. Moschou,[a,1,2] Andrei P. Smertenko,[b,1] Elena A. Minina,[a] Kazutake Fukada,[a] Eugene I. Savenkov,[a] Stephanie Robert,[c] Patrick J. Hussey,[b] and Peter V. Bozhkov[a]**

[a] Department of Plant Biology and Forest Genetics, Uppsala BioCenter, Swedish University of Agricultural Sciences and Linnean Center for Plant Biology, SE-75007 Uppsala, Sweden

[b] The Integrative Cell Biology Laboratory, School of Biological and Biomedical Sciences, University of Durham, DH1 3LE Durham, United Kingdom

[c] Department of Forest Genetics and Plant Physiology, Umeå Plant Science Centre, Swedish University of Agricultural Sciences, 901 83 Umea, Sweden

**Vesicle trafficking plays an important role in cell division, establishment of cell polarity, and translation of environmental cues to developmental responses. However, the molecular mechanisms regulating vesicle trafficking remain poorly understood. Here, we report that the evolutionarily conserved caspase-related protease separase (EXTRA SPINDLE POLES [ESP]) is required for the establishment of cell polarity and cytokinesis in *Arabidopsis thaliana*. At the cellular level, separase colocalizes with microtubules and RabA2a (for RAS GENES FROM RAT BRAINA2a) GTPase-positive structures. Separase facilitates polar targeting of the auxin efflux carrier PIN-FORMED2 (PIN2) to the rootward side of the root cortex cells. Plants with the *radially swollen4* (*rsw4*) allele with compromised separase activity, in addition to mitotic failure, display isotropic cell growth, perturbation of auxin gradient formation, slower gravitropic response in roots, and cytokinetic failure. Measurements of the dynamics of vesicle markers on the cell plate revealed an overall reduction of the delivery rates of KNOLLE and RabA2a GTPase in separase-deficient roots. Furthermore, dissociation of the clathrin light chain, a protein that plays major role in the formation of coated vesicles, was slower in *rsw4* than in the control. Our results demonstrate that separase is a key regulator of vesicle trafficking, which is indispensable for cytokinesis and the establishment of cell polarity.**

## INTRODUCTION

Asymmetric distribution of cellular components defines cell polarity, a fundamental property of all organisms, indispensible for their ability to grow and reproduce (Drubin and Nelson, 1996; Dhonukshe et al., 2008; Asnacios and Hamant, 2012). Due to the sessile nature of plants, their response to developmental and environmental cues requires high plasticity of morphogenetic processes. Furthermore, rigid cell walls limit the range of plant cell responses to internal and external signals involved in the regulation of division plane orientation and the direction of cell expansion. Both cell division and cell expansion are regulated by the phytohormone auxin (Woodward and Bartel, 2005). The physiological activity of auxin is translated through the gradients of its distribution across plant tissues and organs. These gradients are established and maintained by membrane influx and efflux carriers, which are responsible for cell-to-cell auxin transport (Petrásek and Friml, 2009). The direction of gradients is determined by the distribution of the auxin carriers to the sides of the cells, and the pattern of localization asymmetry of these carriers serves as a marker of cell polarity.

The PIN-FORMED (PIN) family of plasma membrane proteins is the most well-studied auxin efflux carriers. PIN proteins are typically asymmetrically organized on the plasma membranes and are more abundant on either the shootward or rootward sides of the cell. Mutations in PINs result in perturbation of the auxin gradients and lead to aberrant development (Dhonukshe et al., 2008; Smith, 2008; Korbei and Luschnig, 2011). The correct distribution of PINs in plant cells relies on protein trafficking pathways throughout the endomembrane system (Boutté et al., 2007; Grunewald and Friml, 2010). During cytokinesis, PINs are secreted to all sides of the cells, resulting in initially apolar localization (Dhonukshe et al., 2008). Thereafter, asymmetric recycling of PINs between shootward or rootward plasma membrane and endosomes leads to the establishment of polarity. Shootward and rootward PIN targeting is regulated by different mechanisms (Kleine-Vehn et al., 2006). The rootward PIN delivery is ARF GEF (for exchange factor of ADP ribosylation factor GTPases) GNOM-dependent and sensitive to microtubule depolymerization drug oryzalin (Michniewicz et al., 2007; Kleine-Vehn et al., 2008a, 2008b, 2009; Rahman et al., 2010), whereas

[1] These authors contributed equally to this work.

[2] Address correspondence to panagiotis.moschou@slu.se.

The authors responsible for distribution of materials integral to the findings presented in this article in accordance with the policy described in the Instructions for Authors (www.plantcell.org) are: Panagiotis N. Moschou (panagiotis.moschou@slu.se) and Peter V. Bozhkov (peter.bozhkov@slu.se).

[C] Some figures in this article are displayed in color online but in black and white in the print edition.

[W] Online version contains Web-only data.

www.plantcell.org/cgi/doi/10.1105/tpc.113.113043

the shootward delivery utilizes an ARF -GEF GNOM- and microtubule-independent pathway (Feraru and Friml, 2008; Kleine-Vehn et al., 2008a). Besides the involvement of exocytic pathways, clathrin-mediated endocytosis plays an essential role in the recycling of PIN proteins during establishment and maintenance of cell polarity (Dhonukshe et al., 2007; Feraru et al., 2012).

Polar localization of PINs is a dynamic process governed by developmental and environmental cues, including cell differentiation and gravitropic stimulation. The changes in PIN localization depend on the modulation of overall balance between endo- and exocytosis, as well as the changes of spatial distribution of endo- and exocytic activities. Vesicle trafficking is tightly linked to the dynamics of the cytoskeleton. Apart from the aforementioned role of microtubules in the rootward targeting of PIN2 (Kleine-Vehn et al., 2008a), polar localization and dynamics of PIN1, PIN2, and PIN3 depends on the dynamics of the actin filament (Kleine-Vehn et al., 2008a). During cytokinesis, microtubules are thought to direct the vesicles toward the newly synthesized cell plate (Van Damme and Geelen, 2008); hence, PIN delivery to and cycling at the newly produced cell edges must be determined by the microtubule organization and dynamics. This implies the existence of a link between the cytoskeleton, vesicle trafficking, and PINs localization during both mitosis and interphase. The molecular mechanisms underlying this link remain largely elusive.

Analysis of *Arabidopsis thaliana* mutants compromised in vesicular trafficking helped to unravel the molecular links between cell polarity and vesicular trafficking (Xu and Scheres, 2005; Jaillais et al., 2007; Nakamura et al., 2012). *radially swollen4* (*rsw4*) is a temperature-sensitive point mutation of the *EXTRA SPINDLE POLE* (*ESP*) gene encoding the caspase-related protease separase (Wu et al., 2010). This mutation results in the production of an altered ESP protein with a single amino acid substitution ($Ala^{603}$ to $Val^{603}$). Knockout (or constant knockdown) of *ESP* is embryo-lethal due to the failure of chromosome disjunction (Liu and Makaroff, 2006), consistent with the evolutionarily conserved role of ESP in daughter chromatid separation (Ciosk et al., 1998; Hauf et al., 2001; Moschou and Bozhkov, 2012). In addition to this canonical function, the defects in anisotropic (i.e., directionally dependent) cell expansion observed in *rsw4* (Wu et al., 2010) implicate ESP in the regulation of cell polarity (Yang et al., 2011). This duality of plant ESP function provides an interesting paradigm to study the role of a protease in the spatiotemporal relationship between karyokinesis and establishment of cell polarity.

Here, we used the weak point mutant allele of *ESP* (i.e., *rsw4*) and inducible *ESP* RNA interference (RNAi) lines to reveal the function of plant ESP in the determination of cell polarity, which would not have been possible if we examined null alleles or constitutive RNAi lines. This phenotypic analysis coupled with live-cell imaging and immunofluorescence microscopy demonstrates that ESP plays an important role in linking membrane protein trafficking with the cytoskeleton and is essential for the asymmetric distribution of PIN2 protein and cytokinesis.

## RESULTS

### ESP Deficiency Leads to Perturbed Auxin Gradient in the Root Tip

The apparent isotropic expansion of root cells in a temperature-sensitive mutant allele of *ESP*, *rsw4* (Wu et al., 2010), implicates ESP in the regulation of cell polarity during postembryonic development. Since the establishment of polarity in plants is governed by directional flow and uneven distribution of auxin, we compared the patterns of auxin response in the root tips of *rsw4* and wild-type plants using the synthetic auxin activity reporter *DR5* promoter (*proDR5*), which is transcriptionally fused to an open reading frame encoding the fluorescent protein Venus (proDR5rev:3xVenus-N7; Heisler et al., 2005). The ectopic auxin response maxima occurred in ~1 and 33% of the wild-type and *rsw4* roots, respectively, after incubation on vertical plates at the restrictive temperature for 24 h (Figure 1A). The first ectopic auxin maxima in the *rsw4* roots were observed 12 h after the temperature shift before any signs of isotropic cell expansion became noticeable.

The response of plants to the gravity vector requires rapid redistribution of auxin flow resulting in alteration of spatial auxin maxima. Gravistimulation of wild-type roots leads to higher level of *proDR5* activity in the outermost cell layer on the side that is perpendicular to the gravity vector (Ottenschläger et al., 2003). Consequently, any defects in the formation of an auxin gradient would impair or delay the gravitropic response. We observed that wild-type roots treated for 12 h at the restrictive temperature and then gravistimulated for 3 or 6 h by changing their orientation with respect to the gravity vector by 90° showed enhanced expression of *proDR5* in the outermost cell layer of the root, accompanied by the root bending response (Figure 1B). The *rsw4* seedlings showed less significant displacement of the auxin maxima within 6 h of gravistimulation and a pronounced delay in the root bending response (Figures 1B and 1C).

Since separase knockouts are embryo-lethal, we examined the gravitropic response in transgenic lines with conditionally suppressed expression of *ESP*, which was accomplished using an RNA hairpin construct under a dexamethasone (DEX)–inducible promoter (*ESP RNAi* lines; see Supplemental Figure 1A online). The hairpin construct harbors a β-glucuronidase reporter (*uidA* gene; *GUS*) also under control of the DEX-inducible promoter, which allows selection of the transgenic lines based on GUS expression in their root tips. Although the uniform expression of GUS was already visible after 2 h of induction with 20 μM DEX (see Supplemental Figure 1B online), a significant decrease of *ESP* mRNA level was detected after 12 h of DEX treatment (see Supplemental Figure 1C online).

Nevertheless, no discernible phenotype was observed after 12 h of induction. The longer induction with DEX phenocopied isotropic cell expansion as was previously observed in *rsw4* roots incubated at the restrictive temperature for 24 to 48 h, albeit causing more severe root and root hair swelling and ectopic root hair formation (see Supplemental Figures 1D to 1F online). The gravitropic response of the *ESP RNAi* lines treated with DEX for 12 h and then gravistimulated for 6 h was significantly delayed (see Supplemental Figure 1G online).

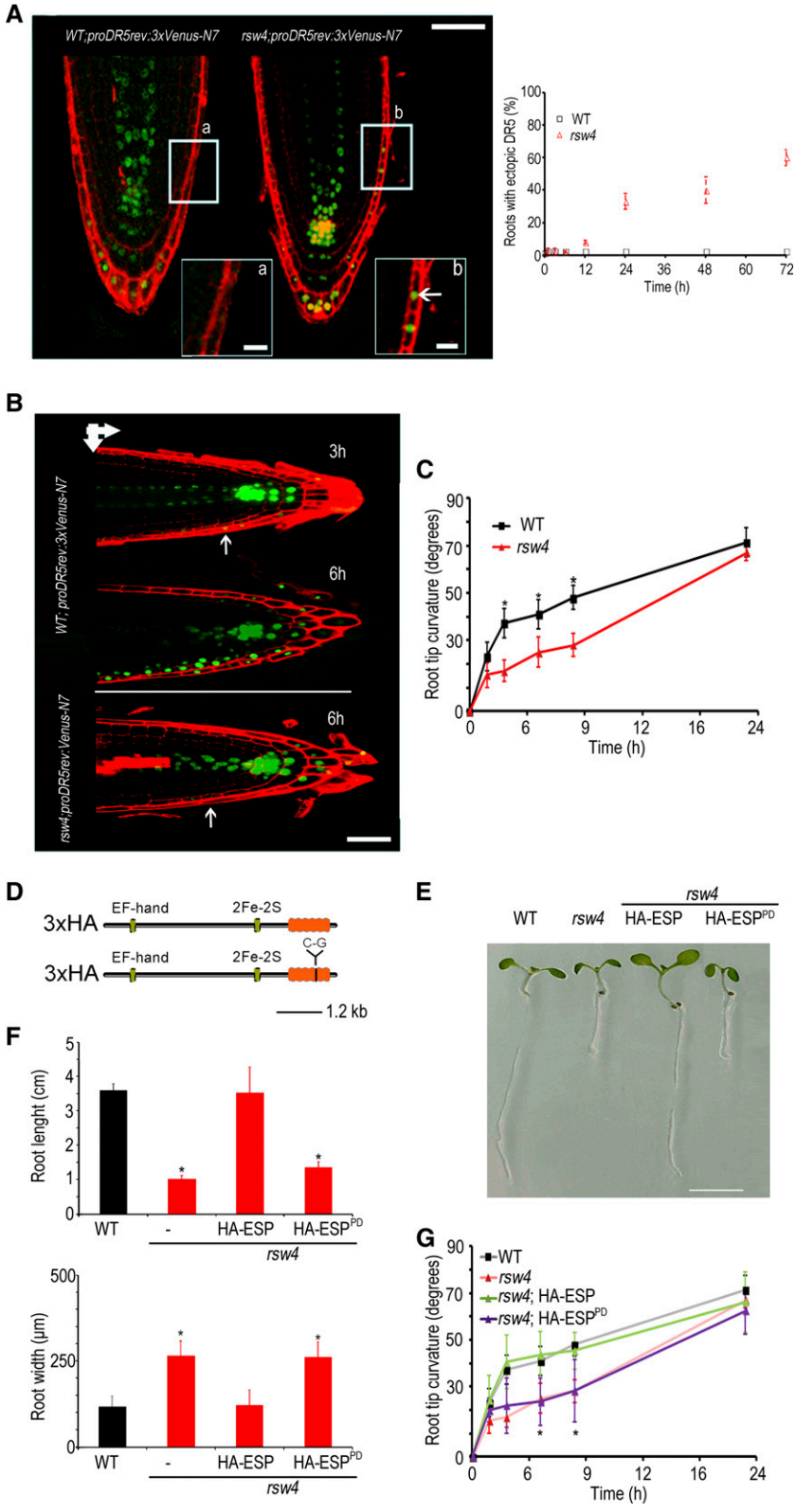


**Figure 1.** ESP Regulates Auxin Response Maxima through Its Proteolytic Activity.

ESP is a Cys protease with a characteristic C-terminal caspase-like catalytic domain containing a conserved dyad of Cys and His (Moschou and Bozhkov, 2012). To investigate whether proteolytic activity of ESP is required for the establishment of an auxin gradient, we introduced a point mutation into the ESP open reading frame to substitute catalytic Cys for Gly ($Cys^{1297}$ to $Gly^{1297}$) in the ESP protein. Subsequently, this mutated *ESP*$^{PD}$ (PD for protease-dead) was introduced into the *rsw4* background (Figure 1D). While *pro35S*:*HA-ESP* fully complemented the temperature-sensitive phenotype of *rsw4* in terms of both root morphology and gravitropic response, the PD version *pro35S*:*HA- ESP*$^{PD}$ could not complement the mutant phenotype (Figures 1E to 1G). Since both *rsw4*;*pro35S*:*HA-ESP* and *rsw4*;*pro35S*:*HA-ESP*$^{PD}$ lines showed a minor increase of ~20% in the *ESP* mRNA level (see Supplemental Figure 1C online), the observed effects could not be attributed to *ESP* mRNA level deregulation. Therefore, catalytic activity of ESP is essential for the establishment of auxin gradient in the root tip as well as the gravitropic response.

### ESP Regulates PIN2 Localization in the Root Cortex

Considering the formation of ectopic auxin response maxima and the perturbed gravistimulation response of *rsw4*, we compared localization of PIN1 and PIN2 proteins in wild-type and *rsw4* plants expressing *proPIN1*:*PIN1-EGFP* (for enhanced green fluorescent protein) and *proPIN2*:*PIN2-EGFP*. The time-course analysis of fluorescence pattern of PIN1-EGFP and PIN2-EGFP fusion proteins in wild-type plants incubated at the restrictive temperature revealed no apparent changes in localization of the proteins during the course of the experiment (96 h). However, in the *rsw4* background, the PIN2-GFP signal on the rootward side of meristematic cortex cells already switched to the shootward side 6 h after incubation at restrictive temperature, while the shootward signal in epidermis and columella cells was not affected (Figures 2A and 2B).

The localization of PIN1 was not affected during 24 h of incubation at the restrictive temperature. Immunostaining of PIN1 and PIN2 in *rsw4* plants incubated at the restrictive temperature for 24 h (Figure 2C) confirmed that endogenous PIN2 polarity in root cortex cells was significantly affected (~60 and 40% of cells showing rootward and shootward localization, respectively) in comparison with the wild type (95 and 5% of cells with rootward and shootward localization, respectively). The polarity of PIN1 was lost after 48 h of incubation at the restrictive temperature coinciding with root swelling (see Supplemental Figure 2 online). These data suggest that this loss of PIN1 polarity is a pleiotropic effect of isotropic cell expansion and perturbed tissue patterning caused by aberrant PIN2 polarity as detected at an earlier time point.

Abnormal PIN localization in *rsw4* under the restrictive temperature could be a pleiotropic effect of mitotic aberrations resulting from *ESP* malfunction. Indeed, staining of roots incubated at restrictive temperature for 72 h with 4′,6-diamidino-2-phenylindole (DAPI) revealed frequent lagging chromatids and unresolved chromosomal bridges (see Supplemental Figure 3A online). However, a significant increase of chromosomal aberrations during the time course experiment in lines expressing histone H2a fused to yellow fluorescent protein (YFP) became apparent only after 36 h of incubation at the restrictive temperature (see Supplemental Figures 3B and 3C online) and coincided with an increase in the frequency of cells with larger nuclei, root tip swelling, and loss of tissue patterning (see Supplemental Figures 3D to 3F online). The loss of correct PIN2 polarity and formation of the ectopic auxin response maxima occurred 30 and 12 h, respectively, before the accumulation of mitotic aberrations, indicating that ESP regulates cell polarity independently of its role in cell division. In addition, since the aberrant PIN2 polarity in cortex cells preceded the root swelling

**Figure 1.** (continued).

**(A)** Localization of DR5:venus promoter activity (bright gray; green online) in the root tips of Col- 0;*proDR5rev*:*3xVenus* (wild type [WT]) and *rsw4*; *proDR5rev*:*3xVenus* (*rsw4*) seedlings, counterstained with propidium iodide (dark gray; red online), and time-course analysis of ectopic maxima accumulation in *rsw4*;*proDR5rev*:*3xVenus*. *rsw4* roots exhibit aberrant pattern of auxin response maxima in lateral columella cells (inset b; arrow). Bars = 65 μm; inset bars = 10 μm. The graph depicts the mean percentage of roots showing auxin response maxima in lateral columella ± SD of triplicate experiments.

**(B)** Localization of DR5:venus promoter activity in root tips of Col-0;*proDR5*:*venus* (WT) and *rsw4*;*proDR5rev*:*3xVenus* (*rsw4*) seedlings, counterstained with propidium iodide, following 3 and 6 h of gravistimulation. Arrowheads in the top left corner denote root orientation before (vertical) and after (horizontal) gravistimulation. Arrows indicate regions where the auxin response maxima are expected. Bar = 65 μm.

**(C)** Time course of root tip curvature in wild-type and *rsw4* seedlings during gravitropic assay. Four days after start of germination, the plates were placed at the restrictive temperature for 12 h, turned by 90°, and incubated under the same conditions for 1.5, 3, 6, 12, and 24 h. The data show mean ± SD of triplicate experiments.

**(D)** The structure of wild-type and catalytically inactive ESP proteins used for complementation of *rsw4*. ESP is 2180 amino acids long with the catalytic domain situated on the C terminus of the protein (right; orange online). Substitution of the catalytic Cys for Gly to yield protease-dead mutant HA-ESP$^{PD}$ is depicted by **(C)** to **(G)**. An EF-hand and a 2Fe-2S motif are ESP specific and cannot be found in any other ESP proteins (Liu and Makaroff, 2006).

**(E)** HA-ESP$^{PD}$ cannot complement the *rsw4* phenotype (short swollen root). Representative image of 7-d-old seedlings incubated at the restrictive temperature for 72 h. Bar = 1 cm.

**(F)** Root length and width in 7-d-old seedlings incubated at the restrictive temperature for 72 h. The data show mean ± SD ($n \geq 60$).

**(G)** Time course of root tip curvature in wild-type, *rsw4*, *rsw4*;*pro35S*:*HA-ESP*, and *rsw4*; *pro35S*:*HA-ESP*$^{PD}$ seedlings during gravitropic assay performed after 12 h incubation at the restrictive temperature. The data show mean ± SD of triplicate experiments.

Asterisks denote values significantly different from the wild type ($P < 0.01$; Student's *t* test). Each experiment included at least 20 seedlings.

[See online article for color version of this figure.]

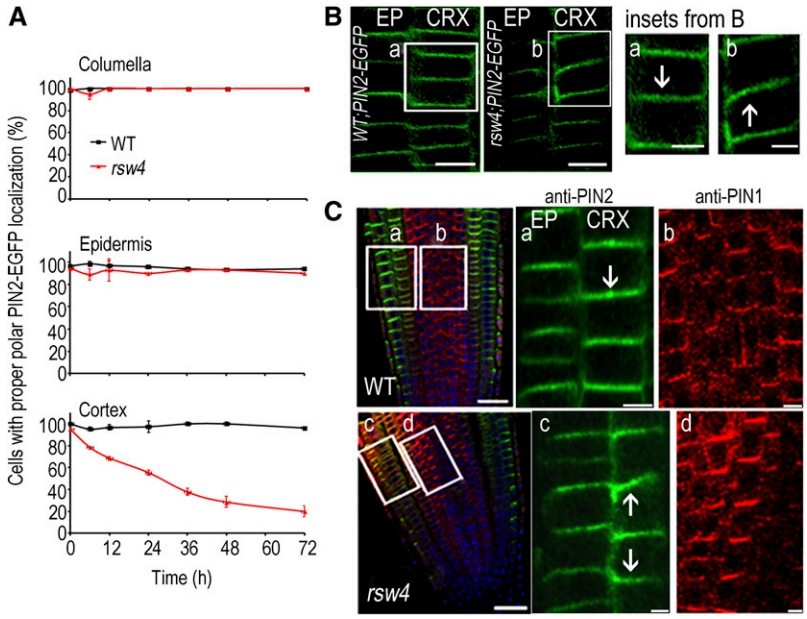


**Figure 2.** ESP Regulates PIN2 Localization.

**(A)** Time-course analysis of PIN2 localization in the columella, epidermis, and cortex cells of the root tips in the *WT*;*proPIN2*:*PIN2-EGFP* (wild type [WT]) and *rsw4*;*proPIN2*:*PIN2-EGFP* (*rsw4*) seedlings during growth at the restrictive temperature. The data show mean ± SD of triplicate experiments.
**(B)** Example of PIN2-EGFP mislocalization (rootward-to-shootward translocation) in the cortex (CRX) cells of *rsw4*. Arrows indicate PIN2-EGFP polarization. Bars = 10 μm (5 μm in insets)
**(C)** Immunostaining of PIN1 (right; red online) and PIN2 (center; green online) in the root tips of wild-type and *rsw4* plants grown at the restrictive temperature. Boxed areas are enlarged and shown to the right. Arrows indicate PIN2 polarization. DNA was stained with DAPI (blue online). Bars = 20 μm (5 μm in insets). EP, epidermis.
[See online article for color version of this figure.]

phenotype by at least 30 h, we conclude that mislocalization of PIN2 is not a pleiotropic effect of aberrant tissue morphology.

The roots from *ESP RNAi* lines, in addition to mitotic aberrations, contained cells with mini-nuclei, reflecting a greater degree of genome instability than in *rsw4* (see Supplemental Figures 3G to 3I online). Similar to *rsw4*, the appearance of cells with abnormal nuclear size in the *ESP RNAi* lines coincided with root swelling, suggesting that the latter could be a consequence of endoreduplication (Wu et al., 2010). Therefore, the lack of *ESP* activity did not block entry into the G1 and S phases, which is concordant with previous observations (Wu et al., 2010).

Pharmacologically induced shootward relocation of PIN2 in the cortex cells affects the *proDR5* activity pattern and suppresses the gravistimulation response (Rahman et al., 2010). Similarly, shootward localization of PIN2 in the root meristematic cortex cells of *rsw4* leads to significant loss of the gravitropic response. Therefore, ESP is an important component of the pathway that regulates rootward targeting of PIN2 in root cortex cells, which is required for the maintenance of the auxin gradient and the gravitropic response.

### ESP Associates with Microtubules and RabA2a-Positive Vesicles

To find out how ESP regulates PIN2 rootward cell polarity, we examined its intracellular localization in wild-type and *pro35S*:*HA-ESP* transgenic *Arabidopsis* roots. During interphase, ESP localized to puncta in the cytoplasm, which may coincide with microtubules (Figure 3A; see Supplemental Figure 4A online, image 1). During cell division, ESP decorates all microtubule arrays including the preprophase band, mitotic spindle, phragmoplast, and cell plate (Figure 3A; see Supplemental Figure 4A online, images 2 to 4). A similar staining pattern was observed in *rsw4*;*pro35S*:*HA-ESP* and *rsw4*;*pro35S*:*HA-ESP*$^{PD}$ lines grown at the restrictive temperature for 24 h (see Supplemental Figures 4B to 4D online). No staining was observed with anti-ESP in *rsw4* plants grown at the restrictive temperature for 12 h, suggesting that temperature shift causes instability of the ESP$^{rsw4}$ allelic protein.

In addition to microtubules, ESP colocalizes with RabA2a-YFP positive compartments, previously shown to define distinct structures in the *trans*-Golgi network/early endosomal compartment (Chow et al., 2008), during both interphase and telophase (Figure 3B and insets; colocalization probability approximately *Pr* = 0.85). Partial colocalization was also found with syntaxin KNOLLE and PIN2-EGFP-positive endosomes at the cell plate (see Supplemental Figures 5A and 5B online). No significant colocalization was observed with Golgi and *trans*-Golgi (see Supplemental Figures 5A and 5B online).

Despite colocalization with microtubules, ESP had no apparent effect on microtubule organization (see Supplemental Figure

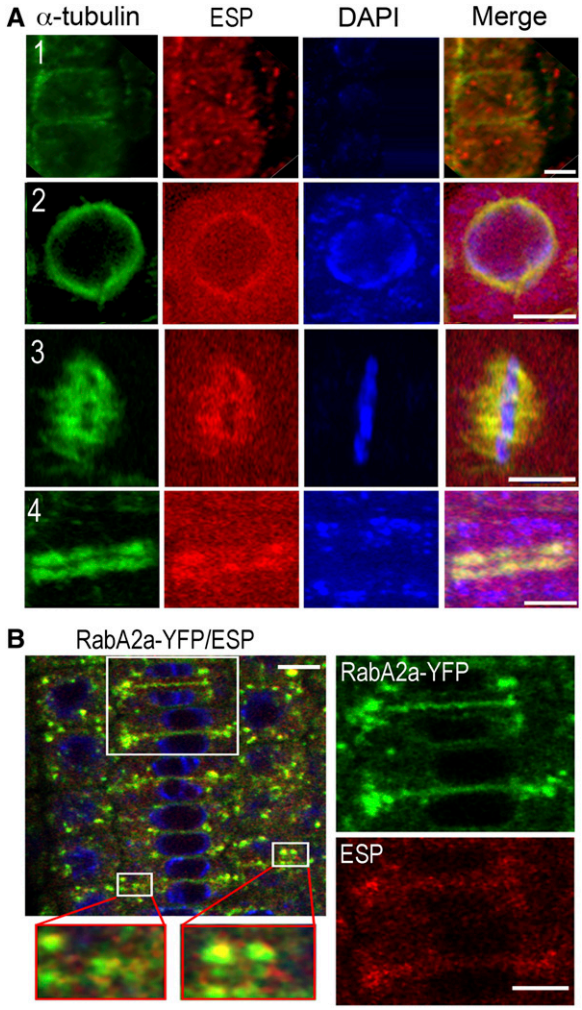


**Figure 3.** Intracellular Localization of ESP.

**(A)** ESP colocalizes with microtubules during interphase (1), prophase (2), metaphase (3), and telophase (4) in the wild-type root tips. Immunostaining with antitubulin (green online, left) and anti-ESP (red), counterstaining with DAPI (blue online), and merging of the images (right). Bars = 5 μm.
**(B)** Colocalization of ESP with RabA2a-positive structures (white; yellow online). Insets indicate enlarged areas. Immunostaining with anti-ESP (red online) and DAPI (blue online) in the root tips of *WT*;*proRabA2a*:*RabA2a-YFP* seedlings (bright gray; green online).
[See online article for color version of this figure.]

6 online; 24 h). Previously, it was suggested that altered microtubule orientations in *rsw4* results from abnormal accumulation of cyclin B1;1 (CYCB1;1) (Wu et al., 2010). Under our conditions, the loss of transverse microtubule arrays in *rsw4* root cells was observed only after 36 h of incubation at the restrictive temperature, long after mislocalization of PIN2 in root cortex cells and formation of ectopic auxin maxima (see Supplemental Figure 6 online). The complete disorganization of microtubules occurred after 48 h of incubation at the restrictive temperature (see Supplemental Figure 6 online). Therefore, mislocalization of PIN2 in root cortex cells seem not to be a consequence of microtubule disorganization, but, conversely, disorganization of microtubules is a result of the pleiotropic effect of perturbed auxin signaling and tissue patterning. These data suggest that ESP acts upstream of microtubules in the regulation of cell polarity.

### The Delivery of PIN2-EGFP to the Plasma Membrane Is Slower in *rsw4*

Colocalization of ESP with RabA2a-positive structures and microtubules suggests that ESP might regulate microtubule-dependent delivery of PIN2 to the rootward plasma membrane in the root cortex cells. To test this hypothesis, we examined the dynamics of PIN2 delivery to the plasma membrane using fluorescence recovery after photobleaching (FRAP) of the entire rootward membrane (Figure 4). The rootward delivery of PIN2-EGFP was significantly slower in cortex cells of *rsw4* compared with the wild type, whereas no difference was detected in epidermal cells (Figures 4A and 4B). The immobile fraction of PIN2-EGFP at the plasma membrane was the same in all samples analyzed, indicating that the slower fluorescence recovery rate of PIN2-EGFP did not result from altered protein retention (Figure 4C). To prove that altered fluorescence recovery of PIN2 was not a pleiotropic effect of the overall reduction of the recycling rate of plasma membrane–associated proteins, we measured the fluorescence recovery rate of the plasma membrane integral protein (PIP2A)-EGFP in the wild type and *rsw4* and found no difference (Figures 4D to 4F). This suggests that ESP deficiency does not cause general membrane trafficking defects, but specifically affects polarized protein delivery. Furthermore, the delivery rates of PIN2-EGFP to the mature cell plate were the same in wild-type and *rsw4* cells, consistent with the view that initial delivery of PIN2-EGFP during cell division is apolar (Men et al., 2008; see Supplemental Figure 7A online). Treatment with the protein synthesis inhibitor cycloheximide (CHX) did not affect the fluorescence recovery rate or the immobile fraction of PIN2-EGFP at the plasma membrane, indicating that *rsw4* does not affect de novo–synthesized PIN2-EGFP rootward delivery (see Supplemental Figure 7B online).

To examine whether lateral diffusion of PIN2-EGFP on the plasma membrane could contribute to the observed differences in the fluorescence recovery rates of wild-type and *rsw4* root cortex cells, we bleached a small area of a PIN2-EGFP–positive rootward plasma membrane (see Supplemental Figure 7C online, samples Control and CHX) and found no difference in fluorescence signal recovery between the wild type and *rsw4*. Next, we repeated the experiment in cells treated with trafficking inhibitors sodium azide and deoxy-D-Glc, which block the energy-dependent trafficking of molecules (Men et al., 2008). Again, the recovery rate of PIN2-EGFP fluorescent signal in the wild type and *rsw4* was indistinguishable, indicating that ESP had no impact on the lateral diffusion of PIN2-EGFP (see Supplemental Figure 7C online, sample CHX-e).

### *rsw4* Is Hypersensitive to Brefeldin A

The recycling of PIN proteins from endosomes to the plasma membrane is sensitive to the fungal toxin Brefeldin A (BFA). BFA inhibits an ARF-GEF GNOM, which regulates intracellular sorting

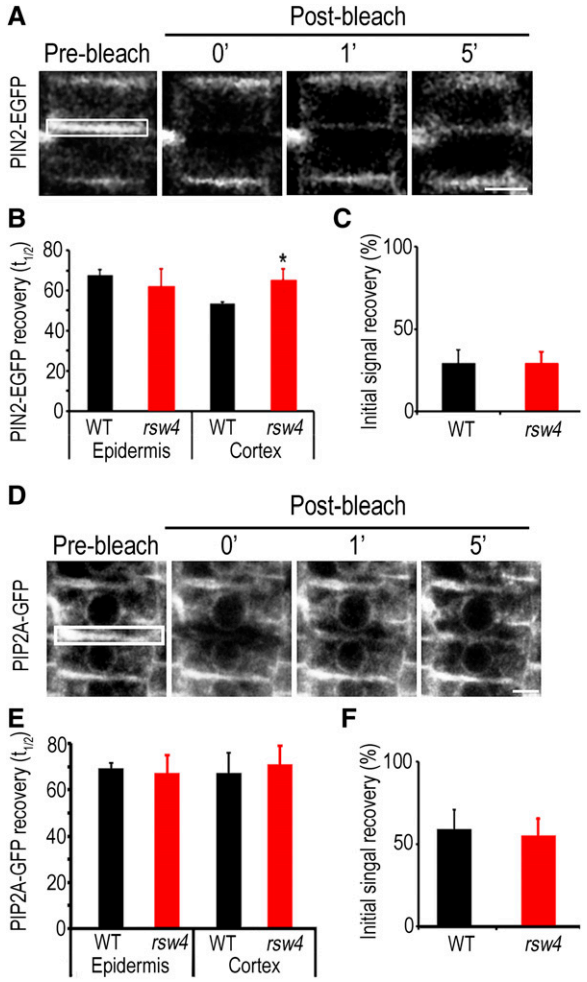


**Figure 4.** ESP Regulates Delivery of PIN2-EGFP Rootward to the Plasma Membrane.

**(A)** Selected time frames (0, 1, and 5 min postbleach) from FRAP analysis of PIN2-EGFP in root cortex cells of *WT*;*proPIN2*:*PIN2-EGFP* (wild type [WT]) and *rsw4*;*proPIN2*:*PIN2-EGFP* (*rsw4*) seedlings. Bar = 5 μm.
**(B)** Recovery rate ($t_{1/2}$) of PIN2-EGFP fluorescent signal in root cortex cells.
**(C)** Percentage of PIN2-EGFP signal recovery in root cortex cells.
**(D)** Selected time frames from FRAP analysis of PIP2A-GFP in root cortex cells of *WT*;*pro35S*:*PIP2-GFP* (WT) and *rsw4*;*pro35S*:*PIP2-GFP* (*rsw4*) seedlings. Bar = 3 μm.
**(E)** Recovery rate ($t_{1/2}$) of PIP2A-GFP fluorescent signal in root cortex cells.
**(F)** Percentage of PIP2A-GFP signal recovery in root cortex cells.
The data show mean ± SD of triplicate experiments, each containing at least 20 seedlings. Asterisks denote values significantly different from the wild type ($P < 0.01$; Student's *t* test). Rectangles in **(A)** and **(D)** indicate the bleached areas.
[See online article for color version of this figure.]

and recycling of PIN1 and PIN2 to the plasma membrane (Geldner et al., 2001; Kleine-Vehn et al., 2008b) and causes accumulation of the proteins in aggregated endosomal compartments (aggresomes). The rootward delivery of PIN2 depends on the ARF-GEF pathway; consequently, rootward localization of PIN2 is more sensitive to BFA than shootward localization (Feraru and Friml, 2008; Kleine-Vehn et al., 2009; Rahman et al., 2010). Furthermore, low concentrations of BFA cause a rootward-to-shootward shift of PIN2 in root cortex cells and perturb the gravistimulation response (Rahman et al., 2010) in the same way as we observed in *rsw4*, implying higher sensitivity of *rsw4* to BFA.

Treatment of wild-type and *rsw4* roots with 50 μM BFA for 1.5 h resulted in internalization of PIN2-EGFP to BFA compartments in both wild-type and *rsw4* (Figure 5A; see Supplemental Figure 8A online), although the internalization occurred more quickly in *rsw4* (see Supplemental Figure 8A online, graph). The effect of BFA is reversible, and localization of PIN2 in the plasma membrane recovers after BFA washout (Geldner et al., 2001). In our experiments, PIN2-EGFP localization in the wild-type cells was almost completely restored as early as only 1 h after washout, while in the *rsw4* cells, PIN2-EGFP positive BFA compartments remained (Figure 5A; see Supplemental Figure 8A online). Furthermore, a similar effect was observed in *ESP RNAi*;*proPIN2*:*PIN2-EGFP* lines (see Supplemental Figure 9 online). To verify that the observed difference was independent of the PIN2-EGFP

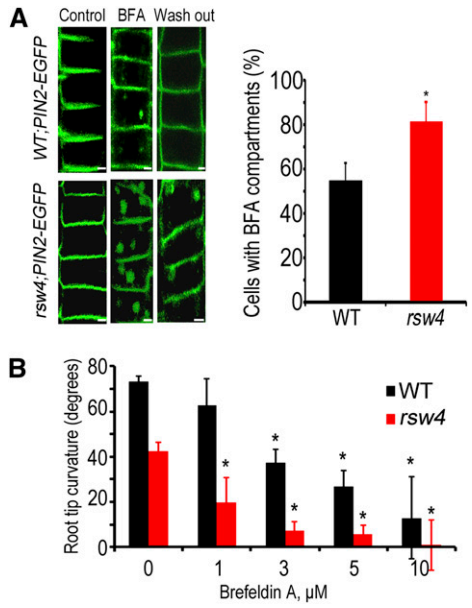


**Figure 5.** *rsw4* Is Defective in BFA-Sensitive Protein Trafficking to the Plasma Membrane.

**(A)** Exocytosis of PIN2-EGFP is perturbed in *rsw4* root cortex cells. Seedlings were incubated for 12 h at the restrictive temperature and then treated with 50 μM BFA for 1.5 h. Cells from untreated roots are designated as Control. BFA-treated roots were washed and incubated for 1 h in liquid MS medium (wash out). Bars = 5 μm. Graph represents percentage of cortex cells with BFA compartments in the wild type (WT) and *rsw4*.
**(B)** Root tip curvature of wild-type and *rsw4* seedlings gravistimulated for 9 h in the presence of BFA. The data from **(A)** and **(B)** show mean ± SD of triplicate experiments, each containing at least 20 seedlings. Asterisks denote values significantly different from the corresponding control ($P < 0.01$; Student's *t* test).
[See online article for color version of this figure.]

degradation rate, wild-type and *rsw4* lines were incubated in the dark for 4 h, and the intensity of the GFP signal was measured in the vacuoles where degradation of PIN2 takes place. The signal was equal in the vacuoles of both the wild type and *rsw4*, indicating that ESP does not affect PIN2 degradation (see Supplemental Figure 8B online). The recovery of PIN2 localization on the plasma membrane after 3 h treatment with BFA followed by 1 h washout occurred only in *rsw4* complemented with the functional *HA-ESP*, but not with the protease-dead mutant *HA-ESP*$^{PD}$ (see Supplemental Figure 8C online).

The gravitropic response of *rsw4* roots was also hypersensitive to BFA. The plants grown on medium supplemented with BFA for 2 d were then incubated at the restrictive temperature for 12 h and subjected to gravitropic stimulation (Figure 5B; Rahman et al., 2010). While ~50% reduction of the gravitropic response was apparent in wild-type seedlings treated with 3 μM BFA, a similar effect in the *rsw4* seedlings was achieved with only 1 μM BFA treatment (Figure 5B). Taken together, the suppressed rootward targeting of PIN2 and the hypersensitivity of *rsw4* to BFA suggest the importance of ESP catalytic activity in the regulation of the ARF-GEF GNOM-dependent PIN2 trafficking pathway.

### Endocytosis Is Not Affected by ESP Failure

In addition to exocytosis, endocytosis plays an important role in the polar localization of PIN2 (Men et al., 2008). To examine whether ESP regulates endocytosis, we measured the overall rate of internalization of the endocytic tracer FM4-64 in wild-type and *rsw4* roots (Ueda et al., 2001; Grebe et al., 2003; Dhonukshe et al., 2007; Men et al., 2008). Pulse labeling with FM4-64 followed by time-lapse imaging of the fluorescent signal in the root epidermis and cortex cells revealed similar dynamics of the appearance of FM4-64–positive endosomes and the net FM4-64 internalization rate in the wild type and *rsw4* (Figures 6A and 6B). Furthermore, no mislocalization of clathrin light-chain-GFP (CLC2-GFP) (Konopka et al., 2008) was observed in the *rsw4* or *ESP RNAi* lines (see Supplemental Figure 10A online, control panels). The changes in CLC2-GFP localization after treatment with the inhibitor of clathrin-mediated endocytosis tyrphostin A23 (Banbury et al., 2003; Konopka et al., 2008) were indistinguishable in the wild-type, *rsw4*, and *ESP RNAi* lines (see Supplemental Figure 10A online, Tyr A23 panels). The inactive analog of tyrphostin A23, tyrphostin A51, had no effect on the localization of CLC2-GFP (see Supplemental Figure 10A online, Tyr A51 panels).

To investigate the role of ESP in endocytosis during cell division, we examined the localization of KNOLLE in wild-type and *rsw4* plants incubated for 12 to 72 h at the restrictive temperature. During cytokinesis, KNOLLE is removed from the lateral cell membranes via DRP1a- (for DYNAMIN RELATED PROTEIN1a) and clathrin-mediated endocytosis, remaining only on the cell plate (Boutté et al., 2010). A significant reduction of endocytosis during cytokinesis would result in the retention of KNOLLE on the lateral membranes. However, no apparent difference in KNOLLE localization was observed between the wild type and *rsw4* (see Supplemental Figure 10B online). Likewise, no apparent difference in KNOLLE localization was observed between wild-type and *ESP RNAi* lines after 12 h induction with DEX (see Supplemental Figure 10B online). We also introduced KNOLLE-GFP into both the wild-type and *ESP RNAi* background and found that after induction with DEX for 24 h or longer, the frequency of cells with KNOLLE-GFP was dramatically reduced in the *ESP RNAi* lines due to the blocking of the transition from metaphase to telophase in all dividing cells (see Supplemental Figure 10C online).

### ESP Regulates the Dynamics of Cell Plate Proteins

Considering the localization of ESP on the phragmoplast microtubules and cell plate after microtubules disassembly, we hypothesized that ESP might be involved in the regulation of vesicular delivery to the cell plate. To investigate this possibility, we performed FRAP analysis of three markers of vesicular compartments (KNOLLE, CLC2, and RabA2a), which accumulate at the cell plate (Lukowitz et al., 1996; Chow et al., 2008; Van

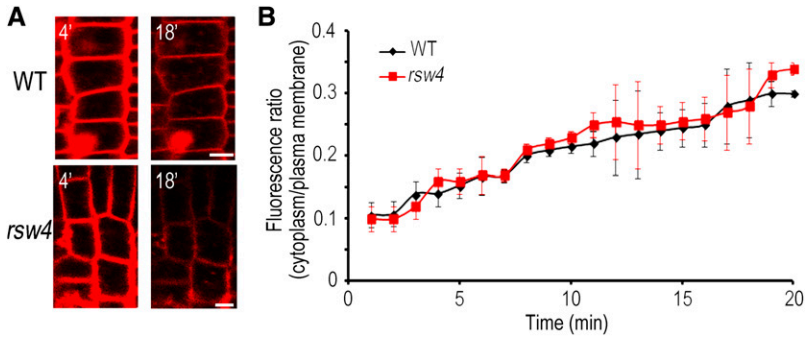


**Figure 6.** Endocytosis Is Not Altered in *rsw4*.

**(A)** FM4-64 internalization in wild-type (WT) and *rsw4* root cells pulsed for 5 min (time 0) and then analyzed during 18 min (time in minutes is shown in the top left corners). Bars = 5 μm.

**(B)** Quantification of FM4-64 internalization rate, as a cytoplasm/plasma membrane ratio of fluorescence in wild-type and *rsw4* root cells. The data show mean ± SD of triplicate experiments, each containing at least 20 seedlings.

[See online article for color version of this figure.]

Damme et al., 2011). The recovery of photobleached fluorescence signal on a region of the cell plate depends on two simultaneous processes: delivery or association of new cytoplasmic molecules and lateral diffusion of preexisting molecules along the cell plate. FRAP on a small region of the cell plate revealed that KNOLLE-GFP had a recovery pattern typical for a protein with lateral diffusion, when recovery depends mostly on preexisting fluorescent molecules diffusing along the cell plate (see Supplemental Figure 11A online). To visualize de novo delivery of new molecules to the cell plate, we excluded the contribution of lateral diffusion by bleaching the whole cell plate. Kymograph analysis revealed that KNOLLE-GFP recovery was random along the cell plate, suggesting that in this case, recovery depends on the delivery of new fluorescent molecules (see Supplemental Figure 11B online). The random recovery pattern was also observed for RabA2a-YFP (see Supplemental Figure 11C online).

The recovery rates (half-times) of all three markers in the wild type were similar at both the permissive and restrictive temperature, and there was no significant difference between values in wild-type and *rsw4* cells measured at the permissive temperature (see Supplemental Figure 12 online). In the apparently nonexpanding cell plates connected to the mother cell walls at the later stages of cytokinesis, the recovery rates of RabA2a-YFP and CLC2-GFP in the *rsw4* roots was ~2 and 7 times slower, respectively, than in the control. The average recovery rate of KNOLLE-GFP was similar to that of the control samples (see Supplemental Figure 12 online). However, we noticed higher standard deviation values than in the case of the former two markers, indicating that association of KNOLLE-GFP with the cell plate is more variable, and this may depend on the stage of cell plate assembly. To address this point, we measured the recovery rates of KNOLLE-GFP during cell plate expansion and observed ~4 times slower recovery in *rsw4* compared with the wild type (Figure 7). This suggests that either additional ESP-independent trafficking pathways are activated to recycle KNOLLE during cell plate maturation or the ESP-dependent pathway is deactivated upon completion of the cell plate expansion. In contrast with KNOLLE, the recovery rates for RabA2a-YFP and CLC2-GFP were similar in expanding and maturing cell plates (see Supplemental Figure 13B online).

Kymographs revealed that CLC2-GFP in *rsw4* lines persisted on the cell plate longer than in the wild type (see Supplemental Figure 11D online). Similar kymographs were obtained in experiments where the FRAP step was omitted (see Supplemental Figure 11D online, -FRAP), indicating that deregulation of ESP causes a delay in maturation and/or detachment of clathrin-coated vesicles. We suggest that ESP regulates trafficking of proteins to the cell plate during the expansion phase and cycling of peripheral membrane proteins during cell plate maturation.

### Deactivation of ESP Results in Cytokinesis Failure

The decreased activity of RabA2a correlates with incomplete cell plate formation in *Arabidopsis* roots (Chow et al., 2008). The perturbation of vesicular trafficking to the expanding cell plate in *rsw4* could result in a slower rate of cell plate expansion and incomplete cell plate formation. We measured the cell plate

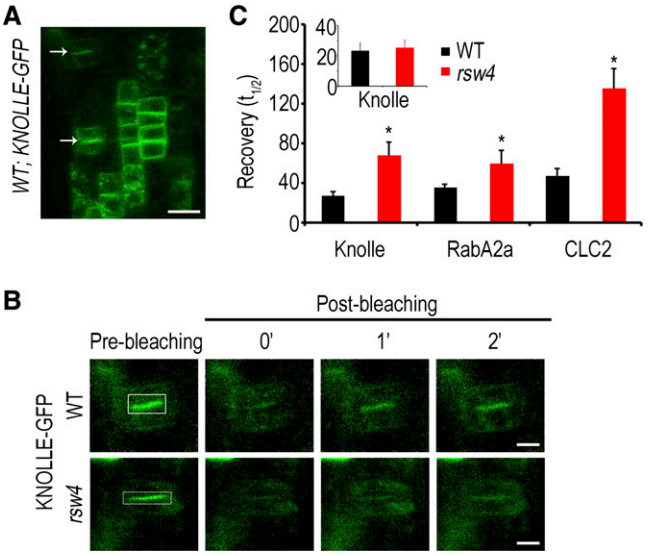


**Figure 7.** ESP Regulates Dynamics of KNOLLE, RabA2a, and Clathrin on the Expanding Cell Plate.

**(A)** Root cells with KNOLLE-GFP–positive expanding cell plates used for analyses, pointed out by arrows. Bar = 10 μm.

**(B)** FRAP analyses of the cell plate–associated fluorescence signal of KNOLLE in the wild type (WT) and *rsw4* at the restrictive temperature. Rectangles indicate the bleached areas. Bars = 2 μm.

**(C)** Recovery rates of fluorescence signal ($t_{1/2}$) of KNOLLE, RabA2a, and clathrin light chain (CLC2) in wild-type and *rsw4* root cells. Inset graph shows KNOLLE recovery at the permissive temperature in the wild type and *rsw4*. The data show mean ± SD of triplicate experiments, each including six or more roots. Asterisks denote values significantly different from the wild type ($P < 0.01$; Student's *t* test).

[See online article for color version of this figure.]

expansion rate by staining cell membranes with FM4-64 and found that, indeed, the expansion rate was significantly reduced in *rsw4* (Figure 8A), while the phragmoplast morphology in *rsw4* and wild-type plants was indistinguishable (see Supplemental Figure 14 online). Kymographs of cell plate expansion in *WT*; *proRabA2a*:*YFP-RabA2a* and *rsw4*;*proRabA2a*:*YFP-RabA2a* plants revealed correct formation of the cell plate leading edges (Figures 8B and 8C). However, YFP-RabA2a signal was homogeneously spread along the cell plate in *rsw4*, compared with more concentrated signal at the leading edges of cell plates in the wild type (Figure 8C, graph). As shown by the immunolocalization experiments, ESP persists at the cell plate following microtubule disassembly, perhaps to regulate maturation events, such as removal of RabA2a proteins, and to reinstate normal vesicular recycling.

Incomplete cell plate formation (cytokinetic failure) was observed in *rsw4* and *rsw4*;*pro35S*:*HA-ESP*$^{PD}$ plants following 12 h incubation at the restrictive temperature (Figure 9, *rsw4*), which is consistent with the role of ESP in the regulation of cell plate assembly. The frequency of cells with cell wall stubs or wavy cell plates was significantly higher in the RNAi lines induced for 12 h (Figure 9, RNAi). Taken together, these data demonstrate that ESP is required for cell plate assembly.

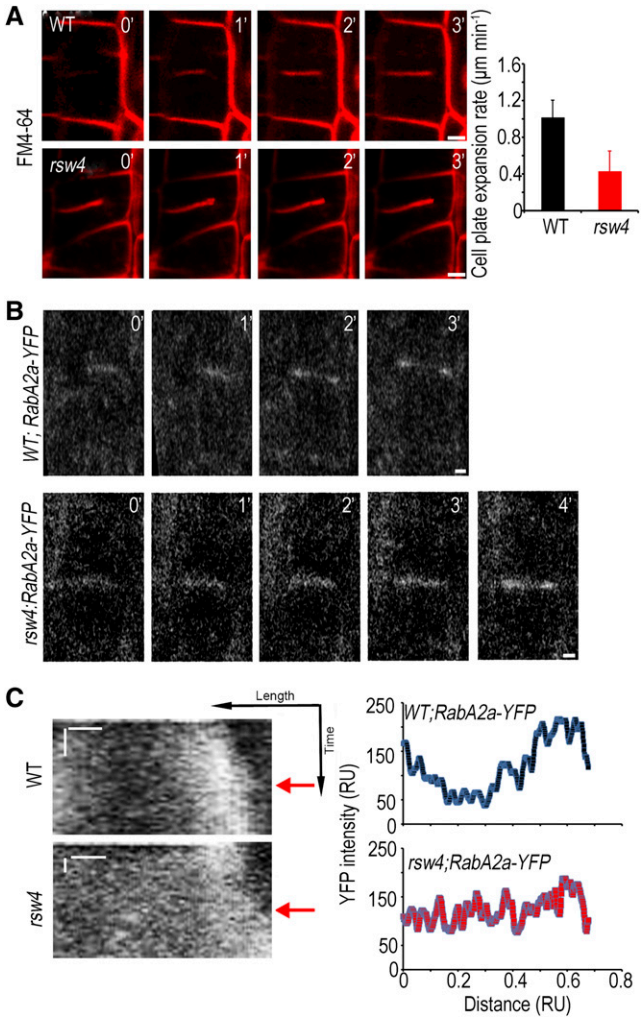


**Figure 8.** ESP Regulates Cell Plate Synthesis.

**(A)** Consecutive time frames showing dynamics of cell plate expansion in wild-type (WT) and *rsw4* seedlings after incubation at the restrictive temperature for 12 h. Staining with FM4-64. The numbers in the top right corners indicate time in minutes. Bars = 2 μm. Graph shows cell plate expansion rate measured in a minimum of six roots ($P < 0.01$; Student's *t* test). Error bars indicate SD.

**(B)** Consecutive time frames of RabA2a-YFP localization on the cell plate in *rsw4*;*proRabA2a*:*RabA2a-YFP* and *WT*;*proRabA2a*:*RabA2a-YFP* seedlings incubated for 12 h at the restrictive temperature. The numbers in the top right corners are minutes. Bars = 2 μm.

**(C)** Kymographs of RabA2a-YFP signal from experiment in **(B)**. Arrows indicate the moment when cell plate fuses to parental cell membrane. Vertical bar = 2 min; horizontal bar = 2 μm. The graphs show RabA2a-YFP signal intensity along the growing cell plate. RU, relative units.

[See online article for color version of this figure.]

## DISCUSSION

Analysis of mutants and pharmacological studies reveal the complexity of signaling networks and the interplay of multiple cellular processes during the establishment of cell polarity. In particular, vesicle trafficking, cell wall synthesis, and the cytoskeleton are known as key players in this process, but what coordinates and brings them together remains unknown. Here, we show that ESP functions in the regulation of cell polarity in *Arabidopsis*. Several lines of evidence support this conclusion. First, compromised ESP activity results in the loss of anisotropic cell expansion and swelling of root cells, including root hairs. Second, there is a delayed gravistimulation response in both the *rsw4* background and inducible *ESP RNAi* lines. Proper gravistimulation response was restored in the *rsw4* background by introducing HA-ESP, while the protease-dead version HA-ESP$^{PD}$ failed to rescue the *rsw4* phenotype, demonstrating that proteolytic activity of ESP is essential for its role in the establishment of cell polarity. Third, perturbation of polar auxin flow in the root tips of *rsw4* was manifested by the appearance of ectopic auxin response maxima and delayed reestablishment of auxin response maxima following gravistimulation. Fourth, localization of PIN2 carrier, which is responsible for the maintenance of the auxin flow, switched from the rootward side of the plasma membrane to the shootward side in the *rsw4* root cortex cells within the meristematic zone.

The localization pattern of ESP points to at least two distinct functions of the protein performed during cell division and during interphase, respectively. Initially, ESP was identified as an executioner of daughter chromatid segregation (Ciosk et al., 1998; Uhlmann et al., 1999). This function requires proteolytic activity of ESP and appears to be conserved in all eukaryotes, from yeasts to vertebrates, as ESP knockouts are lethal in all model systems, including *Arabidopsis* (Liu and Makaroff, 2006; Moschou and Bozhkov, 2012). In agreement with this function, ESP binds to spindle microtubules during prophase, metaphase, and anaphase, to the phragmoplast microtubules, and eventually to the cell plate. In addition, ESP shows transient colocalization with RabA2a-positive structures. The localization of ESP varies across species. For example, yeast ESP associates with spindle poles and anaphase spindle microtubules, whereas human ESP was found only on the spindle poles during metaphase and in the cytoplasm from the onset of anaphase (Jensen et al., 2001; Chestukhin et al., 2003). In the cytoplasm, human ESP was found associated with vesicular compartments of the secretory pathway (Bacac et al., 2011). In *Caenorhabditis elegans*, ESP localizes on spindle poles and chromosomes during metaphase and anaphase and translocates to the cleavage furrow during cytokinesis (Bembenek et al., 2010), where it associates with the cortical granules prior to exocytosis (Bembenek et al., 2007). Therefore, ESP may have another function in the regulation of vesicle trafficking along microtubules, as exemplified by microtubule- and GNOM-dependent targeting of PIN2 to the rootward side of meristematic root cortex cells (Kleine-Vehn et al., 2008a).

Indeed, measurement of PIN2 dynamics at the plasma membrane of root cortex cells by FRAP shows that ESP deficiency leads to slower delivery of PIN2 to the rootward side of the cells. At the same time, ESP has no apparent role in the regulation of lateral diffusion or retention of PIN2 or in PIN2 dynamics at the shootward side of root epidermal cells. GNOM-dependent rootward localization of PIN2 is sensitive to low concentrations of BFA (up to 10 μM) (Rahman et al., 2010), and inhibition of this pathway leads to shootward relocation of PIN2 in the meristematic root cortex cells accompanied by partial loss of the

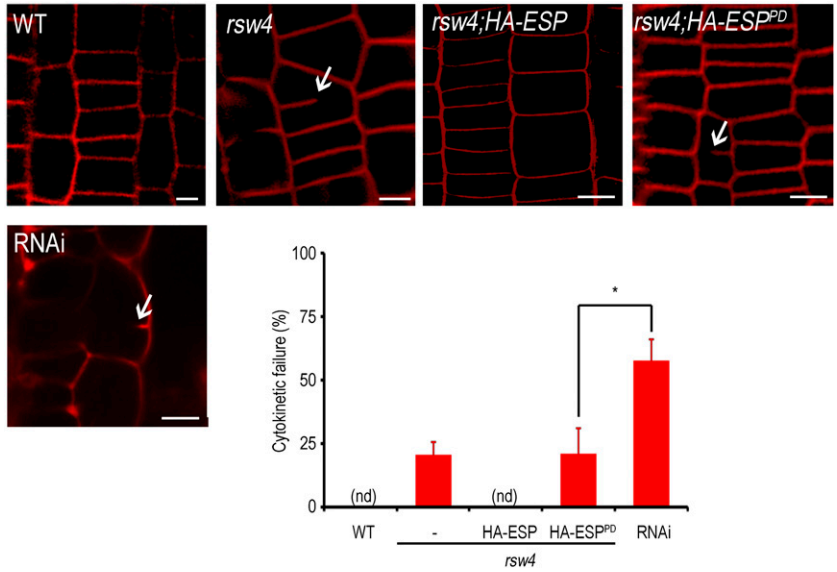


**Figure 9.** Morphology of Cell Plates in the Wild Type and *rsw4*.

Cell wall stubs (arrows) and percentage of postmitotic cells with cell wall stubs (graph) in *rsw4*, *rsw4;pro35S:HA-ESP*, *rsw4;pro35S:HA-ESP*$^{PD}$, and *ESP RNAi* root cells (DEX induced for 12 h). The data on the graph show mean ± SD of triplicate experiments, each including 10 roots. Asterisk denotes that the mean value for *ESP RNAi* was significantly different from that of *rsw4;pro35S:HA-ESP*$^{PD}$ or *rsw4* ($P < 0.01$; Student's *t* test). nd, not detected; WT, the wild type. Bars = 5 μm.

[See online article for color version of this figure.]

gravistimulation response, showing striking similarity to the effect of ESP mutation. Treatment of roots with higher concentrations of BFA induced accumulation of PIN2 in BFA compartments in the cells of both *rsw4* and wild-type plants, but the fluorescence of BFA compartments in *rsw4* was stronger. Similar observations were reported for exocytosis mutants *pp2a* (for *protein phosphatase 2a*) and *bex5/Rab1b* (for BFA-visualized exocytic trafficking defective/RAS GENES FROM RAT BRAINA1b), suggesting that exocytosis is perturbed in *rsw4* (Rahman et al., 2010; Feraru et al., 2012). In agreement with this hypothesis, relocation of PIN2 from the BFA compartments back to the plasma membrane after BFA washout was significantly delayed in *rsw4*. Therefore, we conclude that ESP regulates ARF GNOM and trafficking of PIN2 from recycling endosomes to the rootward plasma membrane.

The polar localization of PIN proteins requires simultaneous activity of both exo- and endocytosis. For example, the reduced rate of endocytosis in the *Arabidopsis cpi1-1* (for *cyclopropylsterol isomerase1-1*) mutant inhibits reestablishment of polar PIN2 localization following cytokinesis (Men et al., 2008). The slower endocytosis in interphase cells leads to a slower internalization rate of the fluorescent dye FM4-64, while during mitosis, defective endocytosis results in localization of the normally cell plate–restricted protein KNOLLE to the lateral sides of the cells (Men et al., 2008). We used both FM4-64 and KNOLLE as markers of endocytic defects (Boutté et al., 2010) and in contrast with *drp1a* and *cpi1-1* found no significant differences between the wild-type, *rsw4*, and *ESP RNAi* lines. Therefore, ESP is unlikely to be a regulator of endocytosis and overall membrane recycling but rather seems to target a specific trafficking pathway different from the ones reported for *drp1a* and *cpi1-1*.

The aberrations of the GNOM-dependent exocytic pathway in *rsw4* may be a consequence of microtubule disorganization. Previously, no changes were reported in the orientation of transverse microtubules in *rsw4* (Wiedemeier et al., 2002), while in a later study, disorganization of microtubules become apparent after 15 h of incubation at the restrictive temperature (Wu et al., 2010). Here, we found no discernible disorganization of cortical microtubules in *rsw4* cells for up to 36 h of incubation at the restrictive temperature, perhaps due to different plant growth conditions. Longer incubations at the restrictive temperature led to disorganization of the cortical microtubule network coincident with a surge in mitotic aberrations, cell swelling, and loss of PIN1 polarity. The loss of transverse microtubule organization might be responsible for the cell swelling; however, what causes disorganization of microtubules is not clear. Wu et al. (2010) suggested that the latter could be a consequence of accumulation of CYCB1;1. Ectopic overexpression of CYCB1;1 in tobacco (*Nicotiana tabacum*) plants causes disorganization of cortical microtubules and cell swelling (Weingartner et al., 2004). Since the accumulation of CYCB1;1 occurred only after 15 h of incubation at the restrictive temperature (Wu et al., 2010), long after the switch of PIN2 polarity, the disorganization of microtubules is more likely to be a downstream effect of the loss of cell polarity and not the cause of the perturbed vesicle trafficking.

Interaction of ESP with microtubules during prophase and metaphase is consistent with its role in orchestrating karyokinesis, but persistence of ESP on the phragmoplast microtubules and association with the cell plate highlights a function of ESP during plant cytokinesis. Multiple components of endo- and exocytic pathways (e.g., KNOLLE, dynamin DRP1A, RabA2a,

exocyst, and clathrin) have been localized to the phragmoplast midzone, providing compelling evidence that vesicle recycling pathways contribute to cell plate assembly (Lukowitz et al., 1996; Van Damme et al., 2006; Chow et al., 2008; Fendrych et al., 2010; Mravec et al., 2011). This conclusion has been further corroborated using mutants of exocytic (KNOLLE; Lukowitz et al., 1996), exocyst (Fendrych et al., 2010), and endocytic (DRP1a; Collings et al., 2008) pathways. The reduced dynamics of KNOLLE, CLC2, and RabA2a at the expanding cell plate and the occurrence of cell wall stubs in *rsw4* and *ESP RNAi* plants indicate that ESP regulates a pathway of vesicle trafficking required for cell plate assembly. During cell plate maturation, the recovery of CLC2 and RabA2a was still significantly reduced, while the recovery of KNOLLE was similar to the control. This suggests that separase regulates vesicle delivery and recycling by several independent pathways: One regulates KNOLLE during the cell plate expansion stage, while different pathway(s) regulate CLC2 and RabA2a. The role of ESP in cytokinesis appears to be evolutionarily conserved, as the *C. elegans* homolog of RabA2a, Rab11, colocalizes with ESP in the cleavage furrow during cytokinesis, and depletion of ESP results in persistence of GFP-Rab11 at the cleavage furrow and the midbody leading to cytokinetic failure (Bembenek et al., 2010). Furthermore, similar to the situation in interphase cells, organization of the phragmoplasts in ESP mutants was indistinguishable from the control, demonstrating that the inhibition of cell plate assembly is not a consequence of microtubule disorganization.

Our data show that the plant homolog of separase, ESP, is essential for three fundamental cellular processes. The first process is daughter chromatid separation during the metaphase to anaphase transition and mitotic progression. The second process is the partitioning of daughter cells during cytokinesis. Unlike the former role, this role may not be evolutionarily conserved and so far has only been clearly demonstrated for *C. elegans* (Bembenek et al., 2010). The third role lies in the establishment and maintenance of cell polarity and tissue patterning. This role is not plant specific either, as the *Drosophila melanogaster* ESP homolog regulates posterior-anterior axis formation during embryogenesis (Rappleye et al., 2002), but its functional conservation in other lineages remains unknown. Considering the apparent endoreduplication events in ESP mutants, ESP does not play a role during the G1 and S phases of the cell cycle (our results; Wu et al., 2010).

The loss of cell polarity in *rsw4* plants takes place within 36 h of incubation at the restrictive temperature and is followed by isotropic cell expansion. This is preceded by the loss of PIN2 polarity after 6 h, appearance of the ectopic auxin response maxima after 12 h, and mitotic failures after 36 h. The isotropic cell expansion is accompanied by disorganization of interphase microtubules and pleiotropic mislocalization of PIN1 protein in the cells after 48 h. This time line demonstrates that the loss of cell polarity does not result from disorganization of cortical microtubules, mitotic failure, and incomplete cytokinesis. In turn, disorganization of cortical microtubules appears to be a consequence of the loss of cell polarity. The swelling of already differentiated cells (e.g., root hairs) at the time of induction of *ESP RNAi* lines further corroborate this conclusion.

In metazoans, the Cys proteases calpains are integral components of the cell polarization machinery (Bórquez and González-Billault, 2011). Being essential for embryogenesis and seed development, plant calpain-like protease Dek1 (for Defective kernel1) has not been implicated in the regulation of cell polarity (Lid et al., 2005). Our work demonstrates that the regulation of cell polarity and cytokinesis in plants is taken over by a member of caspase-related proteases, ESPs, and highlights the evolutionarily conserved role of proteases in the regulation of this process. Since catalytically inactive ESP fails to rescue the *rsw4* phenotype, the regulation of GNOM-dependent recycling of PIN proteins from endosomes to the plasma membrane requires proteolytic cleavage of an as yet unknown substrate(s) by ESP. Identification of the natural targets of ESP will be the next critical step to advance our understanding of the molecular mechanisms coordinating vesicle trafficking and cell polarity.

## METHODS

### Plant Material and Growth Conditions

*Arabidopsis thaliana* plants were grown on vertical plates containing half-strength Murashige and Skoog (MS) medium supplemented with 1% (w/v) Suc and 0.7% (w/v) plant agar, at 20°C (permissive temperature) or 28°C (restrictive temperature), 16/8-h light/dark cycle, and light intensity 150 μE $m^{-2}$ $s^{-1}$. The root swelling phenotype was observed in homozygous *rsw4* plants within 3 d of incubation at 28°C. The following transgenic fluorescent protein marker lines in Columbia-0 (Col-0) background were used: *proRabA2a*:*YFP-RabA2a* (Chow et al., 2008), *p35S*:*GFP-RAB-F2b* (Jaillais et al., 2006), *pro35S*:*N-ST-YFP* and *pro35S*:*NAG1-EGFP* (Grebe et al., 2003), *proPIN1*:*PIN1-GFP* (Benková et al., 2003), *proPIN2*:*PIN2-EGFP* (Xu and Scheres, 2005), and *pro35S*:*GFP-PIP2a* (Cutler et al., 2000). The *proKNOLLE*:*GFP-KNOLLE* was in a Landsberg *erecta*/Niederzens background (Reichardt et al., 2007), *proCLC2*:*CLC2-EGFP* (Konopka et al., 2008) was in Wassilewskija background, and *pro35S*:*smRS-GFP-TUB6*, *pro35S*:*smRS-GFP-TUA6* (Nottingham Arabidopsis Stock Centre; N6550) and *pro35S*:*GFP-TUB9* (Nottingham Arabidopsis Stock Centre; M84706) were in Col-0 background. Gravistimulation assays were performed by incubating plates containing 5-d-old seedlings grown vertically for 12 h under the restrictive temperature and subsequently reorientating the plates by 90° under the same conditions.

### Molecular Biology

All oligonucleotide primers used in this study are shown in Supplemental Table 1 online. *ESP* was amplified by PCR from a cDNA derived from 2-week-old leaves of *Arabidopsis* Col-0 plants. The 5′-end 4.6-kb DNA fragment was amplified using primers FwAtESPExp1topo and RvAtESPdomA and cloned into a pJET vector (Fermentas). The overlapping 3′-end 2.6-kb fragment was amplified by Fw4428AtESP and RvAtESPAscI and then cloned into pJET. The overlapping region contained *Spe*I site. The 5′ fragment was reamplified from pJET by PCR and cloned into the pTOPO/D vector (Invitrogen) giving rise to the pTOPO/D-AtESP 4.6 kb. The remaining part of *ESP* was reamplified by Fw4428AtESP and RvAtESPAscI from the corresponding pJET vector, digested by *Spe*I-*Asc*I, and cloned into *Spe*I-*Asc*I sites of pTOPO/D-AtESP 4.6-kb vector giving rise to full-length clone pTOPO/D-AtESP 6.5 kb. All plasmids and derived constructs were verified by sequencing using the primers AtSE-F1 to AtSE-F9.

For expressing N-terminal HA-epitope tag fusions under the control of 35S promoter, *ESP* was cloned to the destination vectors pGWB615 and pGWB15 (Nakagawa et al., 2007) using Gateway technology (Invitrogen).

Mutations were inserted using the Quickchange Stratagene mutagenesis kit and the primers MutAtSE1 and MutAtSE2 according to the manufacturer's instructions (Stratagene).

For constructing *ESP RNAi* lines, a 435-bp fragment of *ESP* cDNA was amplified using the primers AtESPRNAi2FW and AtESPRNAi2FW. The fragment was introduced by Gateway technology (Invitrogen) to the inducible pOpOff2-KAN vector (Craft et al., 2005).

### Plant Transformation

*Arabidopsis* Col-0 plants were transformed as described previously (Clough and Bent, 1998) using *Agrobacterium tumefaciens* strain GV3101. In all experiments, plants from T2 and T3 generations were used. Transgenic plants were confirmed by PCR.

### Preparation of Antibodies

A 1674-bp-long C-terminal fragment of pTOPO/D-AtESP 6.5 kb was amplified with the primers FwAtESP-dC and RvAtESP-dC, and it was introduced into the entry pDONR/Zeo (Invitrogen) vector using the Gateway BP reaction. Subsequently, the insert was introduced into pDEST-TH1 (Hammarström et al., 2002) and pGAT4 (Ketelaar et al., 2004). The pDEST-TH1-AtESP and pGAT4-AtESP constructs were transformed in BL21 (*DE3*) RIL (Stratagene) *Escherichia coli* cells. Preparation of maltose binding protein (MBP)–tagged recombinant proteins was performed as described previously (Moschou and Roubelakis-Angelakis, 2011). Briefly, protein expression was induced at $OD_{600}$ = 0.5 by adding 0.05 mM to 1 mM isopropyl β-D-1-thiogalactopyranoside to Luria-Bertani medium supplemented with 100 μg $mL^{-1}$ ampicillin and 2 g $L^{-1}$ Glc. The cells were harvested by centrifugation at 2500*g* for 20 min at room temperature and frozen overnight at −80°C. Cells were dissolved in 10 mL of MBP buffer (20 mM Tris, pH 7.4, 400 mM NaCl, 1 mM EDTA, and 0.5 mM PMSF) and lysed at 4°C in a sonicator using four cycles of 15 s to 20 s. Cell debris was removed by centrifugation at 10,000*g* for 20 min at 4°C, and the supernatant was filtered through Miracloth and passed through amylose resin (Biolabs) at 4°C. Protein was eluted using MBP buffer supplemented with 20 mM maltose. Preparation of His-tagged recombinant proteins from pGAT4-AtESP was performed according to the manufacturer's instructions (Qiagen). The antiserum was raised in mice and rabbits using the C-terminal ESP fragment as the antigen.

### Immunocytochemistry and Imaging

*Arabidopsis* roots were fixed for 60 min at room temperature with 4% (w/v) paraformaldehyde in 0.1 M PIPES, pH 6.8, 5 mM EGTA, 2 mM $MgCl_2$, and 0.4% Triton X-100. The fixative was washed away with phosphate buffered saline buffer supplemented with Tween 20 (PBST) and cells were treated for 8 min at room temperature with a solution of 2% (w/v) Driselase (Sigma-Aldrich) in 0.4 M mannitol, 5 mM EGTA, 15 mM MES, pH 5.0, 1 mM PMSF, 10 μg $mL^{-1}$ leupeptin, and 10 μg $mL^{-1}$ pepstatin A. Thereafter, roots were washed twice 10 min each in PBST and in 1% (w/v) BSA in PBST for 30 min and incubated overnight with a primary antibody. The primary antibodies were mouse anti-HA (diluted 1:500), rabbit anti-ESP (1:500), rat anti-tubulin YL1/2 (1:200; Sigma-Aldrich), rabbit anti-KNOLLE (1:1000) (Lukowitz et al., 1996), rabbit anti-PIN1 (1:150), and guinea pig anti-PIN2 (1:150). The specimens were then washed three times for 90 min in PBST and incubated overnight with goat anti-mouse tetramethylrhodamine isothiocyanate or anti-rabbit fluorescein isothiocyanate (FITC) conjugated secondary antibodies diluted 1:200. After washing in the PBST buffer, the specimens were mounted in Vectashield mounting medium (Vector Laboratories).

For plasma membrane staining and endocytosis measurements, seedlings were incubated in liquid half-strength MS medium (LMS; supplemented with 1% [w/v] Suc, pH 5.7) supplemented with 2 μM FM4-64 (Molecular Probes; made from a 2 mM stock in DMSO) for 5 min on ice. The roots were washed two times in ice-cold LMS medium, mounted in LMS medium, and observed immediately.

The samples were examined using Zeiss510, Zeiss710, Zeiss780, or Leica SP5 confocal microscopes.

### Drug Treatments

All drugs were from Sigma-Aldrich, unless otherwise stated. Several 3- to 5-d-old seedlings were submerged in LMS containing corresponding drugs. BFA was dissolved in DMSO and used at 10 μM for 2 h or 50 μM for 1 h. Washout experiments were performed with LMS. Tyrphostin A23 or tyrphostin A51 (Santa Cruz Biotechnology) were dissolved in DMSO and used at 50 μM in LMS for 5 min. CHX was added from a 50 mM aqueous stock to a final concentration of 50 μM. Treatment of seedlings with 0.02% (w/v) sodium azide and 50 mM 2-deoxy-D-Glc was as previously described (Men et al., 2008). Briefly, seedlings were incubated in inhibitor-containing LMS for 30 min and subsequently examined in the presence of the inhibitors. DEX (Sigma-Aldrich) was dissolved in DMSO at 78 mM. Transgene induction was performed on vertical MS plates supplemented with 20 μM DEX.

### Image and Statistical Analysis

The image analysis was done using ImageJ v 1.41 software http://rsb.info.nih.gov/ij/index.html. The kymographs were generated using the ImageJ plug-in written by Jens Rietdorf (FMI, Basel) and Arne Seitz (EMBL, Heidelberg). The recovery rate was calculated by the single exponential fit as described previously (Chang et al., 2005). Colocalization analyses were performed as described previously (French et al., 2008) using Pearson statistics. Spearman analyses gave similar results. Root curvature was measured by Adobe Illustrator v. CS5 (Adobe) on digital photographs. Statistical analysis was performed with SPSS v14 (www.spss.com).

### In Situ GUS Assay

In situ detection of GUS was performed essentially as described earlier (Fincato et al., 2012). DEX-induced *ESP RNAi* roots were stained for 10 min at 37°C, and the intensity of the signal was quantified by densitometry of digital photographs. *ESP RNAi* DEX untreated roots did not show GUS staining even after 2 d of incubation at 37°C.

### Quantitative RT-PCR of ESP mRNA Levels

One hundred root tips were used for each RNA extraction, and 400 ng RNA were used per RT reaction with a Maxima kit (Fermentas, Thermo Fisher Scientific). Out of the list of genes stably expressed throughout developmental stages of *Arabidopsis* (Czechowski et al., 2005), two, *PP2A* (*AT1G13320.1*) and *RNA helicase* (*AT1G58050.1*), were used for normalization (Minina et al., 2013). Quantitative PCR reactions were performed using the iQ5 PCR thermal cycler (Bio-Rad) and DyNAmo Flash SYBR Green qPCR kit (Finnzymes, Thermo Fisher Scientific). For quantification of *ESP* expression, we used the $2^{-\Delta\Delta CT}$ (cycle threshold) method (Livak and Schmittgen, 2001) and three biological replicates.

### Protein Gel Blot Analyses

One hundred milligrams of leaf material was mixed with 100 μL of urea extraction buffer (4 M urea, 100 mM DTT, and 1% [v/v] Triton X-100) and incubated on ice for 10 min. The samples were boiled with Laemmli sample buffer for 10 min and centrifuged at 13,000 rpm for 15 min. Equal amounts of each supernatant were loaded on 10% poly-acrylamide gels

and blotted on a polyvinylidene difluoride (PVDF) membrane. Anti-HA and anti-ACTIN were used at a dilution of 1:1000; anti-rabbit horseradish peroxidase conjugate (Amersham, GE Healthcare) was used at dilution 1:5000. The reaction was developed for 8 h using an ECL Prime kit (Amersham, GE Healthcare) and detected in an LAS-3000 luminescent image analyzer (Fujifilm, Fuji Photo Film).

### FRAP Experiments

Five-day-old seedlings were used for the FRAP experiments. Seedlings were grown on sterile CellView cell culture plates with glass bottoms (35 mm; Greiner Bio One), containing 1 mL of half-strength MS, 1% (w/v) Suc, and 0.3% (w/v) of electrophoresis grade agarose. For inhibitor treatments, plants were placed on plates containing the corresponding inhibitor dissolved in LSM medium. GFP-KNOLLE, RabA2a-YFP, CLC2-GFP, and PIN2-GFP fluorescence was detected using a water- or oil-corrected ×40 objective. During analyses, FRAP mode of Zeiss510meta, Zeiss710 ZEN, or Zeiss780 ZEN software was set up for acquisition of one prebleach image, one bleach scan, and 40 postbleach scans (20 for PIN2-GFP). For FRAP experiments of GFP-KNOLLE over the whole division plane, the width of the bleached region was constant at 2 µm, and the length was adjusted according to the length of each cell plate. The following settings were used for photobleaching: 10 to 20 iterations for GFP-KNOLLE, RabA2a-YFP, and CLC2-GFP and 60 for PIN2-GFP; 10 to 60 s per frame; 100% transmittance with the 458- to 514-nm laser lines of argon laser. Pre- and postbleach scans were at minimum possible laser power (1.4 to 20% transmittance) for the 488 nm and 0% for all other laser lines; 512 × 512 pixel format; and zoom factor of 5.1. Analysis of fluorescence intensities during FRAP was performed in regions of interest (ROIs) corresponding to the size of the bleached region. One ROI was measured outside the bleached region to serve as the background. The fluorescence recovery values were determined, then the background values were subtracted from the fluorescence recovery values, and the resulting values were normalized against the first postbleach time point.

For the analysis of lateral mobility of GFP-KNOLLE, fluorescence recovery values were corrected for the artificial loss of fluorescence using values from the neighboring cells. At least eight cells from different roots were analyzed for each FRAP experiment.

For the analysis of lateral mobility of PIN2-GFP in the cell plate, the photobleached area was set up as a 2-µm rectangle in the middle of the cell plate. Postbleach images were acquired with 20-s intervals over 6 min. After subtraction of background values, the artificial loss of fluorescence in the bleached ROI was corrected using fluorescence signal intensity values measured over the entire cell.

### Accession Numbers

Sequence data from this article can be found in the GenBank/EMBL data libraries under the following accession numbers: *ESP*, AT4G22970; *RabA2a*, AT1G09630; *RabF2b*, AT4G19640; *PIN1*, AT1G73590; *PIN2*, AT5G57090; *PIP2a*, AT3G53420; *Knolle*, AT1G08560; *CLC2*, AT2G40060; *TUB6*, AT5G12250; *TUA6*, AT4G14960; and *TUB9*, AT4G20890.

### Supplemental Data

The following materials are available in the online version of this article.

**Supplemental Figure 1.** Molecular and Phenotypic Analysis of Inducible *ESP* RNAi Lines.

**Supplemental Figure 2.** Abnormal Localization of PIN1 (Red) and PIN2 (Green) in the *rsw4* Roots after Incubation at the Restrictive Temperature for 48 h.

**Supplemental Figure 3.** Mitotic Aberrations and Developmental Defects in *rsw4* and *ESP RNAi* Lines.

**Supplemental Figure 4.** HA-ESP and HA-ESP$^{PD}$ Colocalize with Microtubules.

**Supplemental Figure 5.** Colocalization Analysis of ESP with Microtubules, Golgi, Cell Plate, Late Endosomes, and PIN2.

**Supplemental Figure 6.** Loss of Transverse Orientation of Cortical Microtubule in Root Epidermal Cells of *rsw4*.

**Supplemental Figure 7.** Apolar and Biosynthetic Delivery of PIN2-EGFP Remains Unaffected in *rsw4*.

**Supplemental Figure 8.** Exocytosis of PIN2-EGFP Is Affected in *rsw4*, but the Degradation Pathway Is Normal.

**Supplemental Figure 9.** *ESP RNAi* Lines Are Defective in Protein Trafficking to the Plasma Membrane.

**Supplemental Figure 10.** ESP Deficiency Does Not Affect Clathrin (CLC2) or KNOLLE Localization.

**Supplemental Figure 11.** FRAP and Kymograph Analysis of KNOLLE, Clathrin CLC2, and RabA2a at the Cell Plate.

**Supplemental Figure 12.** FRAP Analyses of KNOLLE, CLC2, and RabA2a in Maturing Cell Plates in the Wild-Type and *rsw4* Samples.

**Supplemental Figure 13.** FRAP Analysis of CLC2 and RabA2a at the Expanding and Maturing Cell Plates in Wild-Type Cells.

**Supplemental Figure 14.** Phragmoplast Structure in Wild-Type and *rsw4* Plants.

**Supplemental Table 1.** List of Primers Used in This Study.

## ACKNOWLEDGMENTS

We thank Tobias Baskin, Markus Grebe, Gerd Jürgens, Ian Moore, Klaus Palme, Tsuyoshi Nakagawa, Sebastian Bednarek, Takashi Ueda, and Thierry Gaude for sharing published research materials. This work was supported by grants from the Swedish Research Council (to P.N.M., S.R. and P.V.B.), from the August T. Larsson Foundation (to A.P.S. and P.V.B.), from the Pehrssons Fund (to P.V.B.), from the Swedish Foundation for Strategic Research (to P.V.B.), from the Olle Engkvist Foundation (to P.V.B.), from VINNOVA (to SR) and from the Knut and Alice Wallenberg Foundation (to S.R. and P.V.B.).

## AUTHOR CONTRIBUTIONS

P.N.M., A.P.S., and P.V.B. designed research. P.N.M., A.P.S., E.A.M., K.F., and E.I.S. performed research. S.R., and P.J.H. contributed new reagents/analytic tools. P.N.M., A.P.S., and P.V.B. analyzed data. P.N.M., A.P.S., and P.V.B. wrote the article.

Received April 23, 2013; revised May 21, 2013; accepted June 7, 2013; published June 28, 2013.

## REFERENCES

**Asnacios, A., and Hamant, O.** (2012). The mechanics behind cell polarity. Trends Cell Biol. **22:** 584–591.

**Bacac, M., Fusco, C., Planche, A., Santodomingo, J., Demaurex, N., Leemann-Zakaryan, R., Provero, P., and Stamenkovic, I.** (2011). Securin and separase modulate membrane traffic by affecting endosomal acidification. Traffic **12:** 615–626.

**Banbury, D.N., Oakley, J.D., Sessions, R.B., and Banting, G.** (2003). Tyrphostin A23 inhibits internalization of the transferrin receptor by perturbing the interaction between tyrosine motifs and the medium chain subunit of the AP-2 adaptor complex. J. Biol. Chem. **278:** 12022–12028.

**Bembenek, J.N., Richie, C.T., Squirrell, J.M., Campbell, J.M., Eliceiri, K.W., Poteryaev, D., Spang, A., Golden, A., and White, J.G.** (2007). Cortical granule exocytosis in C. elegans is regulated by cell cycle components including separase. Development **134:** 3837–3848.

**Bembenek, J.N., White, J.G., and Zheng, Y.X.** (2010). A role for separase in the regulation of RAB-11-positive vesicles at the cleavage furrow and midbody. Curr. Biol. **20:** 259–264.

**Benková, E., Michniewicz, M., Sauer, M., Teichmann, T., Seifertová, D., Jürgens, G., and Friml, J.** (2003). Local, efflux-dependent auxin gradients as a common module for plant organ formation. Cell **115:** 591–602.

**Bórquez, D.A., and González-Billault, C.** (2011). Regulation of cell polarity by controlled proteolytic systems. Biol. Res. **44:** 35–41.

**Boutté, Y., Frescatada-Rosa, M., Men, S.Z., Chow, C.M., Ebine, K., Gustavsson, A., Johansson, L., Ueda, T., Moore, I., Jürgens, G., and Grebe, M.** (2010). Endocytosis restricts *Arabidopsis* KNOLLE syntaxin to the cell division plane during late cytokinesis. EMBO J. **29:** 546–558.

**Boutté, Y., Ikeda, Y., and Grebe, M.** (2007). Mechanisms of auxin-dependent cell and tissue polarity. Curr. Opin. Plant Biol. **10:** 616–623.

**Chang, H.Y., Smertenko, A.P., Igarashi, H., Dixon, D.P., and Hussey, P.J.** (2005). Dynamic interaction of NtMAP65-1a with microtubules in vivo. J. Cell Sci. **118:** 3195–3201.

**Chestukhin, A., Pfeffer, C., Milligan, S., DeCaprio, J.A., and Pellman, D.** (2003). Processing, localization, and requirement of human separase for normal anaphase progression. Proc. Natl. Acad. Sci. USA **100:** 4574–4579.

**Chow, C.M., Neto, H., Foucart, C., and Moore, I.** (2008). Rab-A2 and Rab-A3 GTPases define a trans-Golgi endosomal membrane domain in *Arabidopsis* that contributes substantially to the cell plate. Plant Cell **20:** 101–123.

**Ciosk, R., Zachariae, W., Michaelis, C., Shevchenko, A., Mann, M., and Nasmyth, K.** (1998). An ESP1/PDS1 complex regulates loss of sister chromatid cohesion at the metaphase to anaphase transition in yeast. Cell **93:** 1067–1076.

**Clough, S.J., and Bent, A.F.** (1998). Floral dip: A simplified method for Agrobacterium-mediated transformation of *Arabidopsis thaliana*. Plant J. **16:** 735–743.

**Collings, D.A., Gebbie, L.K., Howles, P.A., Hurley, U.A., Birch, R.J., Cork, A.H., Hocart, C.H., Arioli, T., and Williamson, R.E.** (2008). *Arabidopsis* dynamin-like protein DRP1A: A null mutant with widespread defects in endocytosis, cellulose synthesis, cytokinesis, and cell expansion. J. Exp. Bot. **59:** 361–376.

**Craft, J., Samalova, M., Baroux, C., Townley, H., Martinez, A., Jepson, I., Tsiantis, M., and Moore, I.** (2005). New pOp/LhG4 vectors for stringent glucocorticoid-dependent transgene expression in *Arabidopsis*. Plant J. **41:** 899–918.

**Cutler, S.R., Ehrhardt, D.W., Griffitts, J.S., and Somerville, C.R.** (2000). Random GFP:cDNA fusions enable visualization of subcellular structures in cells of *Arabidopsis* at a high frequency. Proc. Natl. Acad. Sci. USA **97:** 3718–3723.

**Czechowski, T., Stitt, M., Altmann, T., Udvardi, M.K., and Scheible, W.R.** (2005). Genome-wide identification and testing of superior reference genes for transcript normalization in *Arabidopsis*. Plant Physiol. **139:** 5–17.

**Dhonukshe, P., Aniento, F., Hwang, I., Robinson, D.G., Mravec, J., Stierhof, Y.D., and Friml, J.** (2007). Clathrin-mediated constitutive endocytosis of PIN auxin efflux carriers in *Arabidopsis*. Curr. Biol. **17:** 520–527.

**Dhonukshe, P., et al**. (2008). Generation of cell polarity in plants links endocytosis, auxin distribution and cell fate decisions. Nature **456:** 962–966.

**Drubin, D.G., and Nelson, W.J.** (1996). Origins of cell polarity. Cell **84:** 335–344.

**Fendrych, M., Synek, L., Pecenková, T., Toupalová, H., Cole, R., Drdová, E., Nebesárová, J., Sedinová, M., Hála, M., Fowler, J.E., and Zársky, V.** (2010). The *Arabidopsis* exocyst complex is involved in cytokinesis and cell plate maturation. Plant Cell **22:** 3053–3065.

**Feraru, E., Feraru, M.I., Asaoka, R., Paciorek, T., De Rycke, R., Tanaka, H., Nakano, A., and Friml, J.** (2012). BEX5/RabA1b regulates trans-Golgi network-to-plasma membrane protein trafficking in *Arabidopsis*. Plant Cell **24:** 3074–3086.

**Feraru, E., and Friml, J.** (2008). PIN polar targeting. Plant Physiol. **147:** 1553–1559.

**Fincato, P., Moschou, P.N., Ahou, A., Angelini, R., Roubelakis-Angelakis, K.A., Federico, R., and Tavladoraki, P.** (2012). The members of *Arabidopsis thaliana* PAO gene family exhibit distinct tissue- and organ-specific expression pattern during seedling growth and flower development. Amino Acids **42:** 831–841.

**French, A.P., Mills, S., Swarup, R., Bennett, M.J., and Pridmore, T.P.** (2008). Colocalization of fluorescent markers in confocal microscope images of plant cells. Nat. Protoc. **3:** 619–628.

**Geldner, N., Friml, J., Stierhof, Y.D., Jürgens, G., and Palme, K.** (2001). Auxin transport inhibitors block PIN1 cycling and vesicle trafficking. Nature **413:** 425–428.

**Grebe, M., Xu, J., Möbius, W., Ueda, T., Nakano, A., Geuze, H.J., Rook, M.B., and Scheres, B.** (2003). *Arabidopsis* sterol endocytosis involves actin-mediated trafficking via ARA6-positive early endosomes. Curr. Biol. **13:** 1378–1387.

**Grunewald, W., and Friml, J.** (2010). The march of the PINs: Developmental plasticity by dynamic polar targeting in plant cells. EMBO J. **29:** 2700–2714.

**Hammarström, M., Hellgren, N., van Den Berg, S., Berglund, H., and Härd, T.** (2002). Rapid screening for improved solubility of small human proteins produced as fusion proteins in *Escherichia coli*. Protein Sci. **11:** 313–321.

**Hauf, S., Waizenegger, I.C., and Peters, J.M.** (2001). Cohesin cleavage by separase required for anaphase and cytokinesis in human cells. Science **293:** 1320–1323.

**Heisler, M.G., Ohno, C., Das, P., Sieber, P., Reddy, G.V., Long, J.A., and Meyerowitz, E.M.** (2005). Patterns of auxin transport and gene expression during primordium development revealed by live imaging of the *Arabidopsis* inflorescence meristem. Curr. Biol. **15:** 1899–1911.

**Jaillais, Y., Fobis-Loisy, I., Miège, C., Rollin, C., and Gaude, T.** (2006). AtSNX1 defines an endosome for auxin-carrier trafficking in *Arabidopsis*. Nature **443:** 106–109.

**Jaillais, Y., Santambrogio, M., Rozier, F., Fobis-Loisy, I., Miège, C., and Gaude, T.** (2007). The retromer protein VPS29 links cell polarity and organ initiation in plants. Cell **130:** 1057–1070.

**Jensen, S., Segal, M., Clarke, D.J., and Reed, S.I.** (2001). A novel role of the budding yeast separin Esp1 in anaphase spindle elongation: Evidence that proper spindle association of Esp1 is regulated by Pds1. J. Cell Biol. **152:** 27–40.

**Ketelaar, T., Voss, C., Dimmock, S.A., Thumm, M., and Hussey, P.J.** (2004). *Arabidopsis* homologues of the autophagy protein Atg8 are a novel family of microtubule binding proteins. FEBS Lett. **567:** 302–306.

**Kleine-Vehn, J., Dhonukshe, P., Sauer, M., Brewer, P.B., Wiśniewska, J., Paciorek, T., Benková, E., and Friml, J.** (2008b). ARF GEF-dependent transcytosis and polar delivery of PIN auxin carriers in *Arabidopsis*. Curr. Biol. **18:** 526–531.

**Kleine-Vehn, J., Dhonukshe, P., Swarup, R., Bennett, M., and Friml, J.** (2006). Subcellular trafficking of the *Arabidopsis* auxin

influx carrier AUX1 uses a novel pathway distinct from PIN1. Plant Cell **18:** 3171–3181.

**Kleine-Vehn, J., Huang, F., Naramoto, S., Zhang, J., Michniewicz, M., Offringa, R., and Friml, J.** (2009). PIN auxin efflux carrier polarity is regulated by PINOID kinase-mediated recruitment into GNOM-independent trafficking in *Arabidopsis*. Plant Cell **21:** 3839–3849.

**Kleine-Vehn, J., Langowski, L., Wisniewska, J., Dhonukshe, P., Brewer, P.B., and Friml, J.** (2008a). Cellular and molecular requirements for polar PIN targeting and transcytosis in plants. Mol. Plant **1:** 1056–1066.

**Konopka, C.A., Backues, S.K., and Bednarek, S.Y.** (2008). Dynamics of *Arabidopsis* dynamin-related protein 1C and a clathrin light chain at the plasma membrane. Plant Cell **20:** 1363–1380.

**Korbei, B., and Luschnig, C.** (2011). Cell polarity: PIN it down! Curr. Biol. **21:** R197–R199.

**Lid, S.E., Olsen, L., Nestestog, R., Aukerman, M., Brown, R.C., Lemmon, B., Mucha, M., Opsahl-Sorteberg, H.G., and Olsen, O.A.** (2005). Mutation in the *Arabidopsis thaliana* DEK1 calpain gene perturbs endosperm and embryo development while over-expression affects organ development globally. Planta **221:** 339–351.

**Liu, Z., and Makaroff, C.A.** (2006). *Arabidopsis* separase AESP is essential for embryo development and the release of cohesin during meiosis. Plant Cell **18:** 1213–1225.

**Livak, K.J., and Schmittgen, T.D.** (2001). Analysis of relative gene expression data using real-time quantitative PCR and the 2(-Delta Delta C(T)) method. Methods **25:** 402–408.

**Lukowitz, W., Mayer, U., and Jürgens, G.** (1996). Cytokinesis in the *Arabidopsis* embryo involves the syntaxin-related KNOLLE gene product. Cell **84:** 61–71.

**Men, S., Boutté, Y., Ikeda, Y., Li, X., Palme, K., Stierhof, Y.D., Hartmann, M.A., Moritz, T., and Grebe, M.** (2008). Sterol-dependent endocytosis mediates post-cytokinetic acquisition of PIN2 auxin efflux carrier polarity. Nat. Cell Biol. **10:** 237–244.

**Michniewicz, M., et al**. (2007). Antagonistic regulation of PIN phosphorylation by PP2A and PINOID directs auxin flux. Cell **130:** 1044–1056.

**Minina, E.A., Sanchez-Vera, V., Moschou, P.N., Suarez, M.F., Sundberg, E., Weih, M., and Bozhkov, P.V.** (2013). Autophagy mediates caloric restriction-induced lifespan extension in *Arabidopsis*. Aging Cell **12:** 327–329.

**Moschou, P.N., and Bozhkov, P.V.** (2012). Separases: Biochemistry and function. Physiol. Plant. **145:** 67–76.

**Moschou, P.N., and Roubelakis-Angelakis, K.A.** (2011). Characterization, assay, and substrate specificity of plant polyamine oxidases. Methods Mol. Biol. **720:** 183–194.

**Mravec, J., et al**. (2011). Cell plate restricted association of DRP1A and PIN proteins is required for cell polarity establishment in *Arabidopsis*. Curr. Biol. **21:** 1055–1060.

**Nakagawa, T., Kurose, T., Hino, T., Tanaka, K., Kawamukai, M., Niwa, Y., Toyooka, K., Matsuoka, K., Jinbo, T., and Kimura, T.** (2007). Development of series of gateway binary vectors, pGWBs, for realizing efficient construction of fusion genes for plant transformation. J. Biosci. Bioeng. **104:** 34–41.

**Nakamura, M., Kiefer, C.S., and Grebe, M.** (2012). Planar polarity, tissue polarity and planar morphogenesis in plants. Curr. Opin. Plant Biol. **15:** 593–600.

**Ottenschläger, I., Wolff, P., Wolverton, C., Bhalerao, R.P., Sandberg, G., Ishikawa, H., Evans, M., and Palme, K.** (2003). Gravity-regulated differential auxin transport from columella to lateral root cap cells. Proc. Natl. Acad. Sci. USA **100:** 2987–2991.

**Petrásek, J., and Friml, J.** (2009). Auxin transport routes in plant development. Development **136:** 2675–2688.

**Rahman, A., Takahashi, M., Shibasaki, K., Wu, S., Inaba, T., Tsurumi, S., and Baskin, T.I.** (2010). Gravitropism of *Arabidopsis thaliana* roots requires the polarization of PIN2 toward the root tip in meristematic cortical cells. Plant Cell **22:** 1762–1776.

**Rappleye, C.A., Tagawa, A., Lyczak, R., Bowerman, B., and Aroian, R.V.** (2002). The anaphase-promoting complex and separin are required for embryonic anterior-posterior axis formation. Dev. Cell **2:** 195–206.

**Reichardt, I., Stierhof, Y.D., Mayer, U., Richter, S., Schwarz, H., Schumacher, K., and Jürgens, G.** (2007). Plant cytokinesis requires de novo secretory trafficking but not endocytosis. Curr. Biol. **17:** 2047–2053.

**Smith, R.S.** (2008). The role of auxin transport in plant patterning mechanisms. PLoS Biol. **6:** e323.

**Ueda, T., Yamaguchi, M., Uchimiya, H., and Nakano, A.** (2001). Ara6, a plant-unique novel type Rab GTPase, functions in the endocytic pathway of *Arabidopsis thaliana*. EMBO J. **20:** 4730–4741.

**Uhlmann, F., Lottspeich, F., and Nasmyth, K.** (1999). Sister-chromatid separation at anaphase onset is promoted by cleavage of the cohesin subunit Scc1. Nature **400:** 37–42.

**Van Damme, D., Coutuer, S., De Rycke, R., Bouget, F.Y., Inzé, D., and Geelen, D.** (2006). Somatic cytokinesis and pollen maturation in *Arabidopsis* depend on TPLATE, which has domains similar to coat proteins. Plant Cell **18:** 3502–3518.

**Van Damme, D., Gadeyne, A., Vanstraelen, M., Inzé, D., Van Montagu, M.C., De Jaeger, G., Russinova, E., and Geelen, D.** (2011). Adaptin-like protein TPLATE and clathrin recruitment during plant somatic cytokinesis occurs via two distinct pathways. Proc. Natl. Acad. Sci. USA **108:** 615–620.

**Van Damme, D., and Geelen, D.** (2008). Demarcation of the cortical division zone in dividing plant cells. Cell Biol. Int. **32:** 178–187.

**Weingartner, M., Criqui, M.C., Mészáros, T., Binarova, P., Schmit, A.C., Helfer, A., Derevier, A., Erhardt, M., Bögre, L., and Genschik, P.** (2004). Expression of a nondegradable cyclin B1 affects plant development and leads to endomitosis by inhibiting the formation of a phragmoplast. Plant Cell **16:** 643–657.

**Wiedemeier, A.M., Judy-March, J.E., Hocart, C.H., Wasteneys, G.O., Williamson, R.E., and Baskin, T.I.** (2002). Mutant alleles of *Arabidopsis* RADIALLY SWOLLEN 4 and 7 reduce growth anisotropy without altering the transverse orientation of cortical microtubules or cellulose microfibrils. Development **129:** 4821–4830.

**Woodward, A.W., and Bartel, B.** (2005). Auxin: Regulation, action, and interaction. Ann. Bot. (Lond.) **95:** 707–735.

**Wu, S., Scheible, W.R., Schindelasch, D., Van Den Daele, H., De Veylder, L., and Baskin, T.I.** (2010). A conditional mutation in *Arabidopsis thaliana* separase induces chromosome non-disjunction, aberrant morphogenesis and cyclin B1;1 stability. Development **137:** 953–961.

**Xu, J., and Scheres, B.** (2005). Dissection of *Arabidopsis* ADP-RIBOSYLATION FACTOR 1 function in epidermal cell polarity. Plant Cell **17:** 525–536.

**Yang, X., Boateng, K.A., Yuan, L., Wu, S., Baskin, T.I., and Makaroff, C.A.** (2011). The radially swollen 4 separase mutation of *Arabidopsis thaliana* blocks chromosome disjunction and disrupts the radial microtubule system in meiocytes. PLoS ONE **6:** e19459.